PROGRAM

MNC 2016

29th International Microprocesses and Nanotechnology Conference

November 8-11, 2016

ANA Crowne Plaza Kyoto, Kyoto, Japan

Sponsored by
The Japan Society of Applied Physics

In Cooperation with

The Institute of Electrical Engineers of Japan
The Institute of Electronics, Information and Communication Engineers
The Japan Society for Precision Engineering
The Japan Society of Mechanical Engineers
The Japanese Society for Synchrotron Radiation Research
The Japanese Society of Microscopy
The Surface Science Society of Japan
The Vacuum Society of Japan

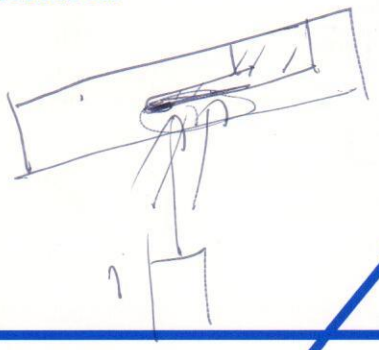

11P-11-66 Electronic Structure of Amorphous WO_{3-x} Thin Film by Soft-X-Ray Spectroscopy T. Sugimoto 1, W. Namiki 1, M. Ochi 1, T. Higuchi 1, T. Tsuchiya 2, M. Minohara 3, M. Kobayashi 3, K. Horiba 3, H. Kumigashira 3 and K. Terabe 2, 1 Tokyo Univ. of Sci., 2 NIMS and 3 KEK, Japan	**11P-11-67** Optical Hydrogen Gas Sensor Consisting of Pd-Loaded Titania Nanocomposite Coating on Flexible Plastic Substrate J. Hamagami, G. Takaya and A. Endo, Kanto Gakuin Univ., Japan	**11P-11-68** A High Performance Microbial Fuel Cell with Nickel Nanoparticle as Cathode Catalyst M. Gebresemati, W.G. Kidanu, S.W. Yoon and H.H. Yoon, Gachon Univ., Korea	**11P-11-69** Synthesis of Ag_3VO_4 Nanoparticles Loaded on Bi_2MoO_6 Nanoplates as Heterostructured Visible Light Driven Photocatalyst A. Phuruangrat, Prince of Songkla Univ., Thailand
11P-11-70 Tuning the Single-molecule Conductance of Extended Metal-Atom Chains by Electrochemical Gating C.H. Chen E.-C. Horng, C.-H. Ho, T.-C. Ting, L.-Y. Hsu, M.-J. Huang, H.-C. Lu, C.-H. Hsu and S.-M. Peng, Natl. Taiwan Univ., Taiwan	**11P-11-71** Effect of Starting Powder Morphology on Film Texture for Bismuth Layer-Structured Ferrolectrics Prepared by Aerosol Deposition Method M. Suzuki, T. Tsuchiya and J. Akedo, AIST, Japan		
Nanoimprint, Nanoprint and Rising Lithography			
Chairperson: M. Okada (Univ. of Hyogo)			
11P-11-72 Development of Multi-Layer Imprint Process for Solid Oxide Fuel Cell K. Tokumaru, F. Tsumori, K. Kudo, T. Osada and K. Shinagawa, Kyushu Univ., Japan	**11P-11-73** Controllable Micro-Optical Element Molds Fabricated by Self-assembly Templating and Metal-Assisted Chemical Etching P. Jin, Y. Han, A. Jin and A. Wang, Harbin Inst. of Technol., China	**11P-11-74** Implementation of a Nanoimprint First Level into Device Fabrication Flows Which Require High Alignment Accuracy S. Pauliac-Vaujour and S. Landis, CEA-LETI, France	**11P-11-75** Large-Scale Patterning Diamond Nanopillar Arrays Using Metal Contact Nanoimprinting W. Zhang 1, Y. Wang 1,2, Y. Wu 1, B. Zhang 1, P. Jin 2, 1 Suzhou Inst. of Nano-Tech and Nano-Bionics and 2 Harbin Inst. of Technol., China
11P-11-76 High-Aspect-Ratio Structure Fabrication by Room-Temperature Nanoimprinting M. Okada and S. Matsui, Univ. of Hyogo, Japan	**11P-11-77** Characteristic Evaluation of Organic Light-Emitting Diodes by Stamp Printing Technique A. Chittawanij and K. Locharoenrat, King Mongkut's Inst. of Technol., Thailand	**11P-11-78** Dependence of Film Thickness on Surface Elasticity and Acrylate Consumption in UV-Cured Thin Film on Au Surfaces H. Yano 1, X. Liang 2, S. Kubo 3, N. Fukuda 4, H. Ushijima 4, K. Nakajima 2 and M. Nakagawa 1, 1 Tohoku Univ., 2 Tokyo Inst. of Technol., 3 NIMS and 4 AIST, Japan	
BioMEMS, Lab on a Chip			
Chairperson: T. Akagi (Univ. of Tokyo)			
11P-11-79 Numerical Investigation of Perforated Polymer Microcantilever Sensor for Contractile Behavior of Cardiomyocytes T.N. Nguyen, D.-W. Lee and B.-K. Lee, Chonnam Natl. Univ., Korea	**11P-11-80** Optical Trapping Dynamics Depend on Initial Assembling of Quantum-Dotconjugated Glutamate Receptors on Hippocampal Neurons T. Kishimoto 1,2, Y. Maezawa 1, S.N. Kudoh 2, T. Taguchi 3 and C. Hosokawa 1,2, 1 AIST, 2 Kwansei Gakuin Univ. and 3 NICT, Japan	**11P-11-81** Thermal Bonding of Polyimide to Form Sealing Microchannels H. Mekaru, AIST, Japan	**11P-11-82** Long-term Perfusion Culture Model of 3D Microvascular Remodeling S. Maeda 1, A. Takano 1, A. Nakamasu 2, R. Yokokawa 3, T. Miura 2 and N. Futai 2, 1 Shibaura Inst. of Technol., 2 Kyushu Univ. and 3 Kyoto Univ., Japan
11P-11-83 Development of Micro-Tube Mass Production Device for Microbial Culture in Open Environment K. Fujimoto, K. Higashi, H. Onoe and N. Miki, Keio Univ., Japan	**11P-11-84** Reduction of Analysis Time in the Size Separation of Large DNA Using Size Exclusion Chromatography-Based Electrophoresis Microchip Driven by Pulsed Electric Field N. Azuma, S. Itoh, K. Fukuzawa and H. Zhang, Nagoya Univ., Japan	**11P-11-85** Rapid and Sensitive Detection of Interleukin-6 with a Sandwich Immunoassay on the Plasmonic Chip K. Tawa 1, M. Sumiya 1, C. Sasakawa 1, T. Sujino 2, H. Nakazawa 2 and M. Umetsu 2, 1 Kwansei Gakuin Univ. and 2 Tohoku Univ., Japan	**11P-11-86** Surface Stress Evaluation Induced by Biomolecular Adsorption on Freestanding Elastomer Nanosheet R. Teramoto 1, T. Fujie 2,3, N. Sato 4, S. Takeoka 4, K. Sawada 1 and K. Takahashi 1,3, 1 Toyohashi Univ. of Technol., 2 Waseda Univ. and 3 JST-PRESTO, Japan
11P-11-87 A Miniaturized Total Analysis System for Real-Time PCR H. Nagai 1, N. Naruishi 1, S. Furutani 1 and T. Fukuzawa 2, 1 AIST and 2 Nippon Sheet Glass, Japan	**11P-11-112L** Proposal of Molecular Tensile Testing by a Centrifugal Microfluidic Approach M. Otake and Y. Ukita, Univ. of Yamanashi, Japan	**11P-11-113L** Cell Migration Control by Boundary Shape of Topographical Structure C. Okutani, A. Wagatsuma, K. Mabuchi and T. Hoshino, Univ. of Tokyo, Japan	**11P-11-114L** Fabrication of Nanoarryas for Exosome Fixation by Lift-off Process and Chemical Modification in Aqueous Solution S. Yokota, H. Kuramachi and T. Ichiki, Univ. of Tokyo, Japan

Numerical Investigation of Perforated Polymer Microcantilever Sensor for Contractile Behavior of Cardiomyocytes

Trieu Khoa Nguyen, Dong-Weon Lee and Bong-Kee Lee
School of Mechanical Engineering, Chonnam National University, 77 Yongbong-ro, Buk-gu, Gwangju 61186, Republic of Korea
Phone: +82-62-530-1685, Fax: +82-62-530-1689, E-mail: b.lee@chonnam.ac.kr

In this study, a numerical investigation of microcantilever sensors for detecting contractile behavior of cardiomyocytes is carried out. Because cardiomyocytes or cardiac muscle cells beat in a periodic manner, there have been several efforts to employ their autonomous motion in developing a novel microsystem or to measure their behavior for investigating biochemical effects of drugs [1, 2]. Recently, a development of novel polymer microcantilever sensor for a preliminary screening of cardiac toxicity was reported [3]. The developed microcantilever sensor was produced to have holes for an easy lift-off from the substrate during the fabrication step. As any geometrical change in the cantilever structure can influence the sensor's performance, effects of the holes should be investigated to obtain a more precise sensing output. In this regard, the numerical model with a simple treatment of surface traction induced by the cardiomyocytes is developed and used to analyze a bending characteristic of the microcantilever.

Figure 1 depicts a schematic of the microcantilever sensor. Because the longitudinal micro-grooves were formed on the top surface where cardiomyocytes were cultured, the cantilever showed the bending motion, which was detected by the external laser displacement sensor. To implement the surface traction on the top surface, the simple numerical model is used as illustrated in Figure 2. C_L and C_U represent lower and upper bounds of the focal area, respectively. It is assumed that a constant surface traction (5 $nN/\mu m^2$ [4] in this specific case) is applied within this area. The periodic surface contraction assigned on the top surface produces an upward bending of the cantilever, like the real experiment.

Three representative geometrical models are used in this study, as shown in Figure 3. It should be noted that Figure 3(c) represents the virtual model for a comparative study. Figure 4 shows the surface traction distributions when C_L and C_U are assigned to be 0.0 and 1.0, respectively. In these cases, the entire surface is assumed to be covered with the cardiomyocytes aligned in the longitudinal direction and length of the single cell is assumed to be 100μm. The contractile surface traction on the top surface produces the asymmetric deformation of the cantilever, resulting in the upward bending as shown in Figure 5. The perforated cantilever results in a reduced bending due to the decreased total surface force even though the holes lowers a stiffness of the cantilever, from 0.125 N/m to 0.108 N/m. As shown in Figure 6, the bending of the cantilever becomes larger as the focal area increases. For all cases, the total surface force exhibits the larger effect than stiffness does. The current numerical model can be utilized in designing microcantilever sensors for cardiomyocytes or investigating cell's behaviors.

Acknowledgement
This work was supported by the International Collaborative R&D Program through the Korea Institute for Advancement of Technology grant funded by the Ministry of Trade, Industry and Energy (N0000894) and Basic Science Research Program through the National Research Foundation of Korea (NRF) funded by the Ministry of Science, ICT & Future Planning (NRF-2014R1A1A1008487).

References
[1] Y. Tanaka, K. Morishima, T. Shimizu, A. Kikuchi, M. Yamato, T. Okano, and T. Kitamori, Lab Chip **6**, 230 (2006).
[2] J. Park, J. Ryu, S. K. Choi, E. Seo, J. M. Cha, S. Ryu, J. Kim, B. Kim, and S. H. Lee, Anal. Chem. **77**, 6571 (2005).
[3] J. Y. Kim, Y.-S. Choi, B.-K. Lee, and D.-W. Lee, Biosens. Bioelectron. **80**, 456 (2016).
[4] N. Q. Balaban, U. S. Schwarz, D. Riveline, P. Goichberg, G. Tzur, I. Sabanay, D. Mahalu, S. Safran, A. Bershadsky, L. Addadi, and B. Geiger, Nat. Cell Biol. **3**, 466 (2001).

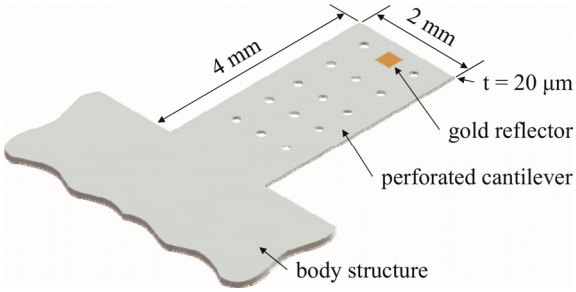

Fig. 1 Schematic diagram of the present microcantilever sensor.

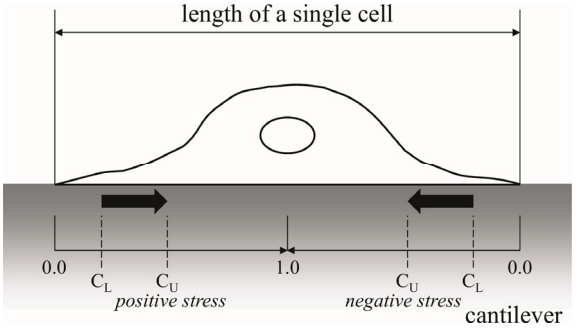

Fig. 2 Model describing the contraction force within a single cell.

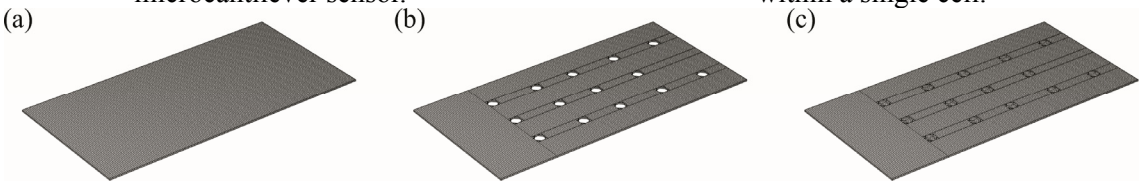

Fig. 3 Finite element meshes for (a) plain cantilever, (b) perforated cantilever, and (c) plain cantilever with confined cells cases.

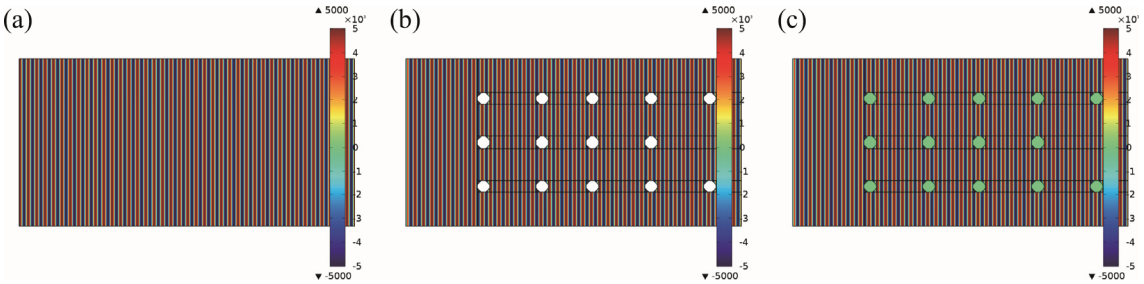

Fig. 4 Surface traction distributions for (a) plain cantilever, (b) perforated cantilever, and (c) plain cantilever with confined cells cases.

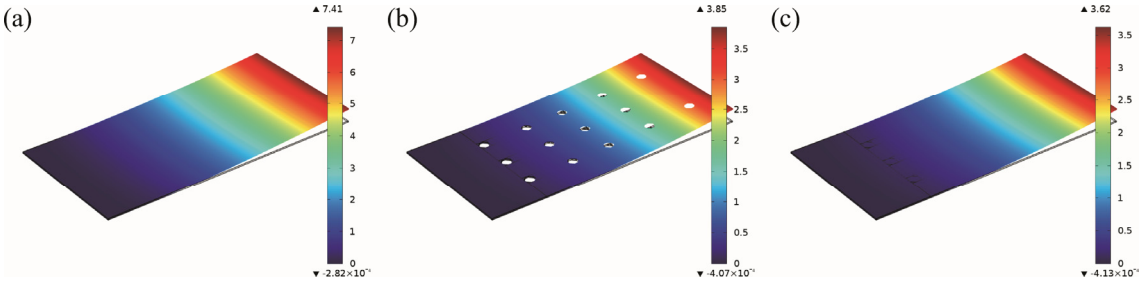

Fig. 5 Deformed cantilevers for (a) plain cantilever, (b) perforated cantilever, and (c) plain cantilever with confined cells cases.

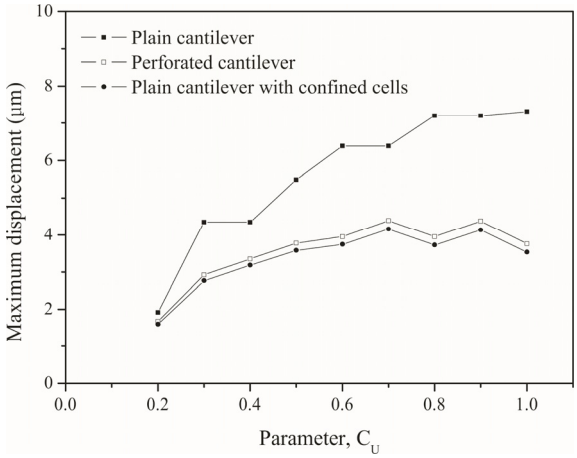

Fig. 6 Effect of model parameter C_U on the maximum displacement (C_L=0.0).